2013

Computational approximation of nonlinear unsteady aerodynamics using an aerodynamic model hierarchy

Mehdi Ghoreyshi
U.S. Air Force Academy

Adam Jirasek
U.S. Air Force Academy

Russell M. Cummings
USAF Academy

Aerospace Science and Technology 28 (2013) 133–144

Contents lists available at SciVerse ScienceDirect

Aerospace Science and Technology

www.elsevier.com/locate/aescte

Computational approximation of nonlinear unsteady aerodynamics using an aerodynamic model hierarchy

Mehdi Ghoreyshi *,[1], Adam Jirásek [1], Russell M. Cummings [2]

Modeling and Simulation Research Center, U.S. Air Force Academy, USAF Academy, CO 80840-6400, United States

ARTICLE INFO

Article history:
Received 14 February 2012
Received in revised form 27 September 2012
Accepted 8 October 2012
Available online 1 November 2012

Keywords:
Reduced order modeling
Unsteady aerodynamics
Computational fluid dynamics

ABSTRACT

Modeling nonlinear unsteady aerodynamic effects in the simulation of modern fighter aircraft is still a very challenging task. A framework for approximating nonlinear unsteady aerodynamics with a Radial Basis Function neural network is provided. Training data were generated from a hierarchy of aerodynamic models. At the highest level, solutions of the discretized Reynolds-Averaged Navier–Stokes (RANS) equations provide the quantitative and qualitative solution of flow around aircraft, although the results are expensive in terms of computational resources. The Euler simulations are less expensive and provide qualitative data up to moderate angles of attack. The integration of these data is promising for generating accurate aerodynamic models at moderate computational cost. To illustrate the method, an airfoil undergoing pitching and plunging motion is considered. The primary and secondary aerodynamic model data are computed using RANS and Euler equations, respectively. A description for a mapping between the aerodynamic loads and the motion parameters based on the implicit function theorem is described. The mapping is then augmented by adding the secondary data to the input dataset. The selection of training data is then discussed. Once the network is trained, it can compute the unsteady aerodynamic loads from motion descriptions on the order of a few seconds. The framework is examined for different motions, and in all cases, the ROM predictions closely represent the actual aerodynamic responses. It is also demonstrated that the aerodynamic hierarchy aids in the rapid development of a reduced-order model.

1. Introduction

The flight mechanics simulation of aircraft requires the evaluation of aerodynamic forces and moments acting on the aircraft, which in general depends on: (1) configuration geometry, (2) vehicle attitude, (3) Mach number, (4) Reynolds number, and (5) angular rates [51]. Bryan [5] was the first who formulated the aerodynamic loads as a function of the instantaneous values of the aircraft's motion state variables and paved the way for subsequent analysis of aircraft flight dynamics [34]. The dependence of the forces and moments on these variables is expanded in a Taylor series, using the first derivatives only and truncating higher-order terms [1]. These assumptions were later questioned based on studies of unsteady aerodynamics by Wagner [60], Küssner [30], Sears [48], and Cowley and Glauert [7]. For example, Wagner [60] showed that for an airfoil undergoing a step change in the angle of attack, there is a time lag until the lift reaches the steady-state value. This time lag cannot be predicted using Bryan's model because the quasi-steady lift change is synchronized with the angle of attack change. Bryan's initial model was later modified to include acceleration derivatives to somehow model the effects from the rate of change of incidence and sideslip angles in time, although this modified model cannot predict the unsteady forces and moments of a rapid maneuvering aircraft in the presence of shock waves and vortical flows [16]. Indeed, the unsteady aerodynamic forces and moments not only depend on the instantaneous states but also their time histories [57,58]. Unfortunately, this makes the aircraft equations of motion an infinite-dimensional problem, where the current states depend on the evolution of previous states at infinitely many points in time [34]. It is essential in practice to reduce the problem dimensions using a Reduced Order Model (ROM) between state-space and aerodynamic loads.

A reduced-order method allows us to describe the unsteady flow in the form of a small number of spatial/temporal modes (typically less than one hundred) compared with the very large number of grid points in the full-order model (on the order of 5 to 50 million or more) [53,35]. Recent efforts on the development of ROMs can be classified into two types: time domain or frequency domain approaches [37]. The frequency domain models are obtained from matching transfer functions computed from

* Corresponding author.
E-mail addresses: Mehdi.Ghoreyshi@usafa.edu (M. Ghoreyshi), Adam.Jirasek@gmail.com (A. Jirásek), Russ.Cummings@usafa.edu (R.M. Cummings).
[1] NRC Research Fellow.
[2] Professor of Aeronautics.

1270-9638/$ – see front matter
http://dx.doi.org/10.1016/j.ast.2012.10.009

Nomenclature

a	acoustic speed	m/s	
c	airfoil chord	m	
$C_{L\alpha}$	lift curve slope	1/rad	
C_L	lift coefficient, $L/q_\infty S$		
C_m	pitching moment coefficient, $m/q_\infty Sc$		
C_N	normal force coefficient, $N/q_\infty S$		
f	frequency	Hz	
h	vertical displacement	m	
H	plunge amplitude	m	
k	discrete time instant		
k	reduced frequency, $\omega c/2V$		
L	lift	N	
m	pitching moment	N m	
M	Mach number, V/a		
N	normal force	N	
p	pressure	Pa	
q_∞	dynamic pressure	Pa	
Re	Reynolds number, $\rho V c/\mu$		
S	wing area	m^2	
s	normalized time, $2Vt/c$		
t	time	s	
v_0	aircraft initial velocity	m/s	
v_a	aircraft reference point velocity	m/s	
V	velocity	m/s	
u	system input vector		
x	system internal states		
y	primary output vector		
y_c	secondary output vector		
Greek			
α	angle of attack	rad	
α_A	pitch amplitude	rad	
α_{eff}	effective angle of attack, $\tan^{-1}(\dot{h}/V)$	rad	
α_s	motion starting angle of attack	rad	
ω	circular frequency	rad/s	
ρ	density	kg/m^3	
μ	air viscosity		
θ	pitch angle	rad	

the measured input–output data [25]. Examples of frequency domain ROMs are the indicial response method by Ballhaus and Goorjian [4] and Tobak et al. [56,55] and a frequency-domain model based on Proper Orthogonal Decomposition (POD) by Hall et al. [24]. The time domain models are obtained by matching time histories of measured data. Some examples of time domain ROMs include the unit sample response by Gaitonde and Jones [15], Volterra theory by Silva and Bartels [49], Radial Basis Functions (RBF) [28] and state-space modeling [20]. Time-domain-based neural networks have also been used to model unsteady aerodynamics [44,38,11,10]. Olcer et al. [44] used neural networks for modeling the unsteady aerodynamic responses to a trailing edge flap deflection and to extract a linear time-invariant model of the flap actuator. Marques and Anderson [38] used a temporal neural network to approximate the unsteady lift and pitch moment of a 2D airfoil for changes in angle of attack in the transonic regime. However, in their model, the network outputs depend on time histories of angle of attack only and not previous values of lift and pitch moment. Faller and Schreck [10] also used a neural network to predict the time-dependent surface pressures of a pitching wing. The network inputs included the instantaneous pitch angle, angular velocity, and the initial surface pressure coefficients at t_0. The network output then predicted the surface pressures at time $t_0 + \Delta t$. These predictions were fed back as the input to the network to predict surface pressures at the next time. This process continues with time until it reaches the final time. However, this model does not have the time histories of motion variables, therefore it might not have sufficient information for modeling highly unsteady flows [19]. In this paper, we use a Radial Basis Function neural network and a mapping between the aerodynamic loads and time histories of both motion parameters and loads based on the implicit function theorem.

There are only limited experimental measurements available to identify the unsteady aerodynamic characteristics used in ROMs. This is mainly due to the complexity of unsteady flow and the limitations of existing test facilities [23]. An alternative is to use simulations based on Computational Fluid Dynamics (CFD). The CFD methods now provide relatively accurate numerical predictions for simulation of unsteady nonlinear aerodynamic problems of maneuvering aircraft [12,14,42,13,26]. At a high level, solutions of the discretized Reynolds-Averaged Navier–Stokes (RANS) equations provide the quantitative and qualitative solution of flow around the aircraft. However, using RANS to develop a model for stability and control analysis is computationally very expensive since such a model needs a large number of time-dependent simulations for different values of motion frequency and amplitude. Fortunately, a range of fluid modeling levels are available, from Reynolds-averaged Navier–Stokes down to potential flow models. Each of the levels has a range of validity and computational cost. For example, potential flow methods are limited to low angles of attack but are computationally inexpensive. Integration of low-cost data indicating trends and a small number of high-cost simulations correcting values helps to reduce the cost of the ROM development. The combination of low and high cost measurement data is also known as multi-fidelity or variable-fidelity methods and have already been established for approximating aerodynamic loads under steady-state conditions [17,47]. However, these approaches are not applicable to predicting unsteady loads where the current loads depend on the past histories of input and output variables.

This paper focuses on the problem of approximating the nonlinear unsteady aerodynamics using a Radial Basis Function Neural Network (RBFNN) using CFD. The first objective of the paper is to find a mapping between aerodynamic loads and input parameters. The test case, geometry definition and ROM are then detailed. The paper continues to describe the generation of training data followed by the assessment of ROM predictions for new generated motions.

2. Formulation

2.1. Problem definition

We consider the problem of approximating the unsteady aerodynamic loads by learning an input–output mapping from a set of m_1 primary and m_2 secondary training data, where $m_2 \gg m_1$ and secondary data are substantially cheaper to collect than the primary data [17]. The first step in solving this problem is to show that a mapping exists between the input vector (including angle of attack and reduced frequency) and the unsteady aerodynamic loads.

The nonlinear and unsteady aerodynamics can be viewed as a multi-input/multi-output dynamic system with a mathematical model in state space given by an ordinary differential equation

$$\dot{x}_t = f(x_t, u_t) \tag{1}$$

and an output equation as:

$$y_t = h(x_t) \tag{2}$$

with given initial condition $x = x_0$, for $t = t_0$ and

$$x_t \in \mathbb{R}^n, \qquad y_t \in \mathbb{R}^m, \qquad u_t \in \mathbb{R}^r$$

where x is an n-dimensional vector of internal state variables over the field $\mathbb{R}$ of real numbers, u is a vector of the inputs to system, and y is an m-dimensional vector of system outputs. For a discrete-time dynamical systems, the equations change to

$$\begin{aligned} x_{k+1} &= f(x_k, u_k) \\ y_k &= h(x_k) \quad \text{for } k = 0, 1, \ldots \end{aligned} \tag{3}$$

where k is an integer value showing discrete time values. The state function f is a smooth function that maps the current state x_k and the input u_k into a new state x_{k+1}, and the output function h maps the state x_k into the output y_k given as [3]

$$f : \mathbb{R}^n \times \mathbb{R}^r \mapsto \mathbb{R}^n, \qquad h : \mathbb{R}^n \mapsto \mathbb{R}^m$$

In this system, the outputs can be determined from the states at time instant k only, therefore the past history of the system is irrelevant [2]. If the state variables are directly measured, the functions f and h can be approximated using neural networks or surrogate-based models. However, in many practical situations, measuring all state variables is limited. Referring to the unsteady aerodynamic problem, the discretized governing equations of fluid dynamics serve as the state space functions with an internal state vector of (ρ, p, u, v, w, E) that corresponds to the values of density, pressure, velocity components, and energy at each grid point. This large amount of data makes the identification of Eq. (3) a very complex task. Fortunately, there are available methods that allow us to reconstruct the state space model by mapping only the input and output data.

For a finite-time interval and a system described by Eq. (3), Levin and Narendra [33] used the Implicit Function theorem [29] to write the output vector at any instant as a function of the past n values of the inputs and the past n values of the outputs, i.e.:

$$y_{k+1} = \Psi(y_k, y_{k-1}, \ldots, y_{k-n+1}, u_k, u_{k-1}, \ldots, u_{k-n+1}) \tag{4}$$

In Eq. (4), Ψ is a vector-valued nonlinear function that maps the inputs to the outputs, and n is an integer representing the past values in the output and input. Eq. (4) preserves the characteristics of the state-space model but no longer depends on system internal states. The input–output mapping, Ψ, can be learned using neural networks when input and output time histories are available. This network is often named a recurrent neural network [2], where the network output becomes part of the next input vector [11]. The remaining problem is how to choose n such that the reconstructed model accurately represents the state-space model described by Eq. (3). The reconstructed model exactly matches Eq. (3) in a neighborhood of the equilibrium state by setting n at most to $2r + 1$, where r is the input vector dimension [9]. In this paper the value of n is selected using "trial and error" attempts.

Having established an input/output mapping for nonlinear unsteady aerodynamics, we now extend the mapping function to allow for primary and secondary measurements. Assume secondary measurements of $\tilde{y}_t \in \mathbb{R}^m$ are also available. These data are assumed to be cheaper to measure than primary data and hence they are available for a larger input vector, $\tilde{u}_t$. Then we define an additional mapping between this system input and secondary data, i.e.

$$\tilde{y}_{k+1} = \tilde{\Psi}(\tilde{y}_k, \tilde{y}_{k-1}, \ldots, \tilde{y}_{k-n+1}, \tilde{u}_k, \tilde{u}_{k-1}, \ldots, \tilde{u}_{k-n+1}) \tag{5}$$

where the secondary output function $\tilde{y}$ is defined as $\tilde{y} = C_j(t)$ for $j = [L, D, m]$ corresponding to lift, drag, and pitch moment. For pitching and plunging oscillations, the secondary input vector includes:

$$\tilde{u}(t) = \big(\alpha(t), \dot{\alpha}(t), \ddot{\alpha}(t)\big) \tag{6}$$

The mapping in Eq. (5) is then used to predict secondary output values at the n past values of the primary input vector, u. The function in Eq. (4) is then augmented by this evaluation in the form of

$$\begin{aligned} y_{k+1} = \Psi(&y_k, y_{k-1}, \ldots, y_{k-n+1}, u_k, u_{k-1}, \ldots, u_{k-n+1}, \tilde{y}_k, \tilde{y}_{k-1}, \\ &\ldots, \tilde{y}_{k-n+1}) \end{aligned} \tag{7}$$

Such a model brings the information of secondary data into the mapping function. In this paper, the aerodynamic force and moment coefficients are considered as the outputs. It is assumed that the drag force changes with time histories of the input vector are small compared with lift and pitch moment in the considered flight conditions, and therefore we limit ourselves to lift force and pitch moment coefficients, i.e. $y = [C_L, C_m]$. The unsteady aerodynamic coefficients are investigated for a number of training maneuvers, such that their motion description defines the input vector. The training data include both Euler and RANS calculations at appropriate conditions.

2.2. Selection of the training maneuvers

A training maneuver(s) is needed to provide enough information to learn the mapping between input and output of the full-order model given by Eq. (4). Previous studies to generate training maneuvers for aerodynamic characteristics [41,21,45,43,40] are limited by the range of the motion frequency content. A ROM identified from such a maneuver has limitations with respect to Stability and Control (S&C) applications. Thus, the basic requirement for a training maneuver to generate a reliable ROM in S&C applications is that it sufficiently covers the desired regressor space of state variables. A ROM built on data produced by such motions can then be used to predict the aircraft aerodynamic behavior within the regressor space. The systematic coverage of the regressor space can be, in general, treated as an optimization problem, with strong constraints resulting from the fact that some axes of the regressor space do not represent an independent variable.

For the current study, we consider an airfoil performing pitching and plunging motions. This defines the amplitudes and frequencies as the input variables. Design Of Experiment (DOE) methods [50,46] are often used to select N_T combinations of these variables for training purposes. For example, Glaz et al. [19] used Latin Hypercubic Sampling (LHS) [39] to select 450 training maneuvers to model aerodynamic loads of a pitching and plunging airfoil at different Mach numbers. An alternative to DOE methods is the design of special training maneuvers that help to effectively cover the parameter space and reduce the number of simulations and hence the total computational cost [28]. Some examples are: linear-frequency chirp, spiral, and Schroeder maneuvers defined in Table 1, with some examples shown in Fig. 1.

In Table 1, α_0 and A denote the starting angle and amplitude of motion, respectively, t is time, and $\omega = 2\pi f$ is the angular velocity. The Schroeder maneuver has three parameters that enable direct control of regressor space coverage. These are amplitude, A, the maneuver length, T, and the number of frequencies in the maneuver, N. In this paper, we use chirp pitching and plunging motions as training maneuvers. These maneuvers are an oscillation with linearly increasingly frequency and are described as:

$$\theta(t) = \theta_A \cos\big(\omega_\theta t^2\big), \qquad h(t) = H \cos\big(\omega_h t^2\big) \tag{8}$$

where, θ_A and ω_θ are the pitch amplitude and rotational velocity, respectively, h is the vertical placement of the airfoil, H is

Table 1
Special training maneuvers: definitions.

Maneuver	Definition
Linear-frequency chirp	$\alpha(t) = \alpha_0 + A\sin(\omega t^2)$
Spiral	$\alpha(t) = \alpha_0 + At\sin(\omega t)$
Schroeder	$\alpha(t) = \alpha_0 + A\sum_{k=1}^{n}\sqrt{\frac{1}{2N}}\cos(\frac{2\pi kt}{T} - \frac{\pi k^2}{N})$

the plunge amplitude, and ω_h denotes the oscillatory frequency. The reduced frequencies, k_θ and k_h are defined as $\omega_\theta c/2V$ and $\omega_h c/2V$, where c is the airfoil chord and V is the velocity. Regarding these motions, the input vector is defined as

$$u(t) = [k_\theta, k_h, h, \theta] \tag{9}$$

The chirp by its definition eliminates the need of repeating motions for different values of reduced frequency and amplitudes. However, for the CFD generation of data, these motions start from a steady solution at an initial angle of attack and speed, and run for a time step and a given moment reference point (one might include these additional variables to the input vector). In this paper, six training data sets were generated: three chirp plunge and three chirp pitch, each starting at different angles of attack. Now, we detail the method of RBF neural networks for approximating the function Ψ given in Eq. (4).

2.3. RBF neural networks reduced-order model

Radial Basis Function Neural Networks (RBFNN) are considered as nonlinear input–output models that have been found very useful for multivariate scattered data interpolation [6]. RBFNN provides an approximation of the functions based on the location of data points, and is generally much faster than multi-layer feed-forward neural networks [2]. Given an input vector of $\{X_j^c:\ j = 1,\ldots,p\}$, $X_j^c \in \mathbb{R}$ and a corresponding output vector of $\{Y_j^c:\ j = 1,\ldots,p\}$, $Y_j^c \in \mathbb{R}$, the RBF approximates the output at a new given point as:

$$\hat{Y}(X^*) = \sum_{k=1}^{P} \alpha_k \Phi_k(X) \tag{10}$$

such that

$$\hat{Y}(X_j^c) = Y_j^c, \quad \text{for } j = 1, 2, \ldots, p \tag{11}$$

where α_k are the weights of the linear combiners. The functions Φ_k are named Radial Basis Functions and are often described by a Gaussian basis function as:

$$\Phi_k(X) = \exp\left(-\frac{\|X^* - X_j^c\|^2}{\beta^2}\right) \tag{12}$$

where, β is a real variable to be chosen by the user, and $\|.\|$ denotes the Euclidean norm such that the functions Φ_k will vanish at sufficiently large values of $\|X^* - X_j^c\|$. In terms of the network structure, the RBFNN is a two-layer processing structure with one hidden layer that approximates Φ_k at each node. Then, the output layer is a set of linear combiners of approximation from hidden layer nodes. The network is then trained to minimize the error between the target (desired) values and the network predicted values.

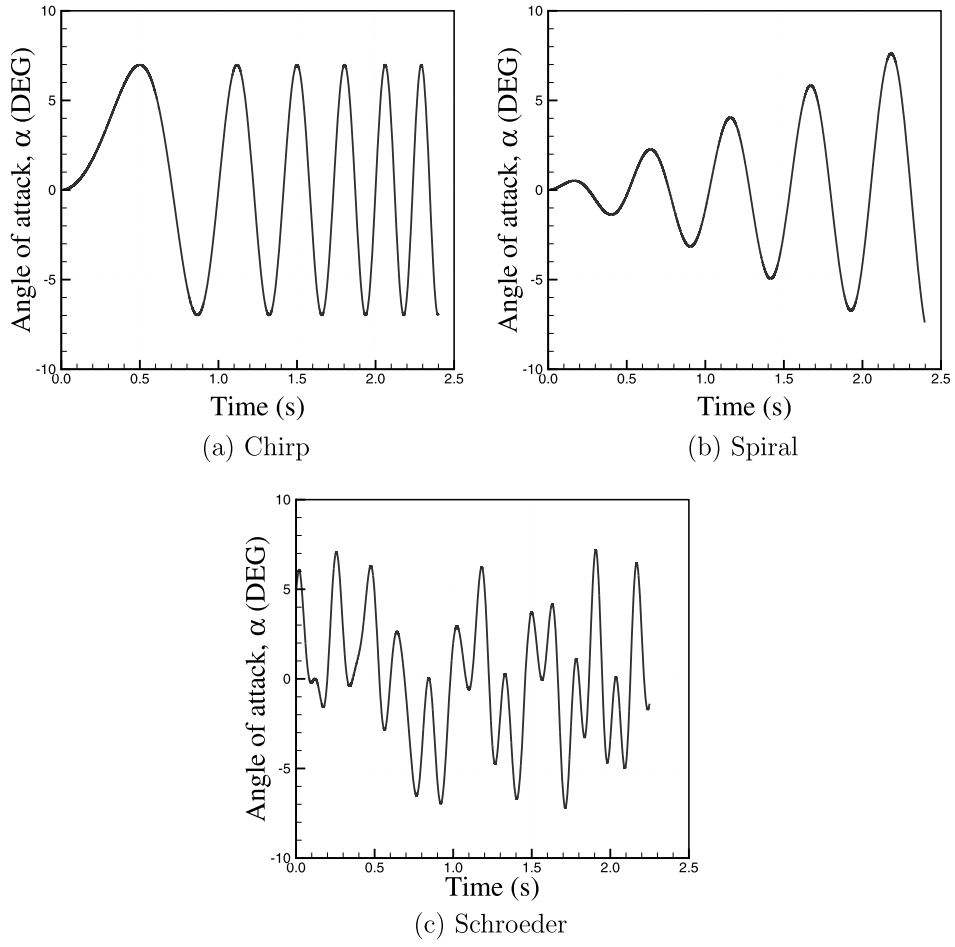

Fig. 1. Special training maneuvers.

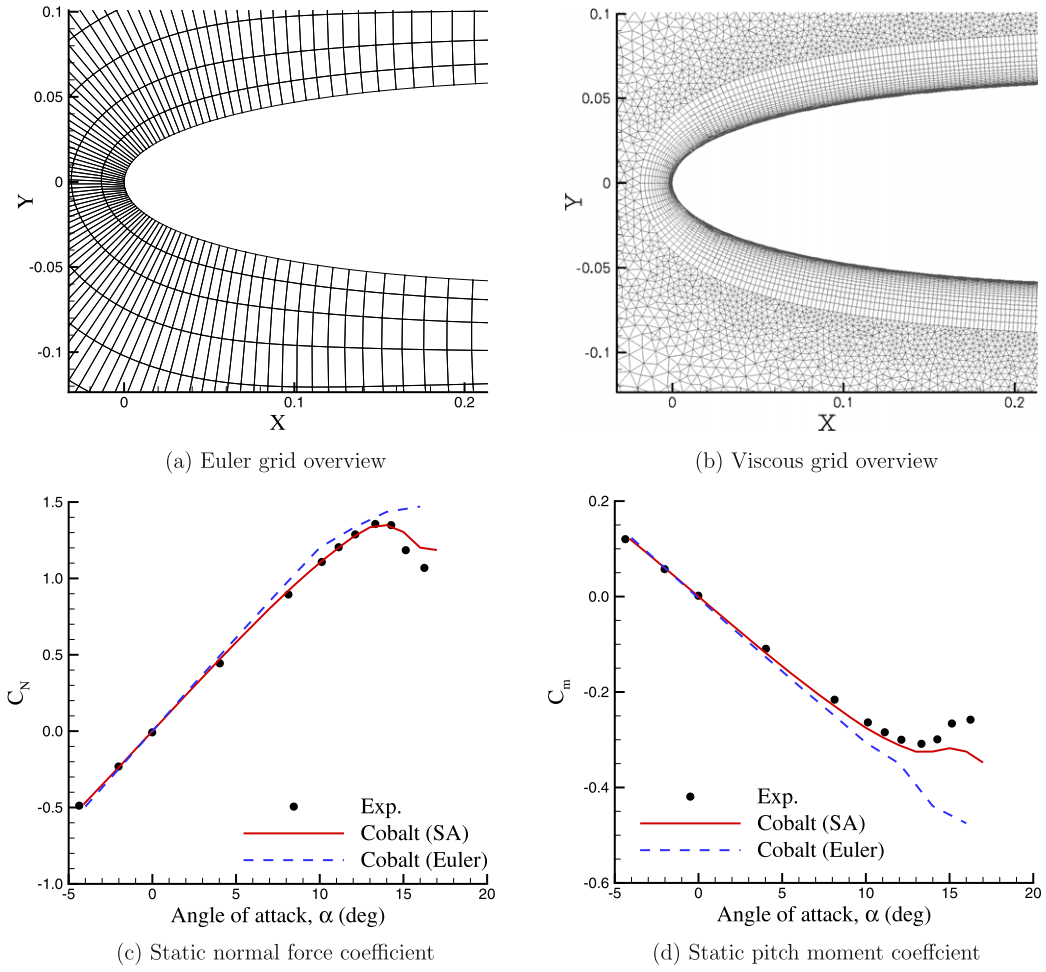

(a) Euler grid overview (b) Viscous grid overview

(c) Static normal force coefficient (d) Static pitch moment coeffcient

Fig. 2. The NACA 0012 grids and static validation. Figures (a) and (b) show the Euler and RANS grids, respectively. The static conditions are: $M_\infty = 0.3$ and $Re = 5.93 \times 10^6$. Experiments are shown with filled circles [31], the solid and dashed lines show the *Cobalt* RANS and Euler predictions, respectively.

2.4. CFD solver

The flow solver used for this study is *Cobalt* [54], which solves the unsteady, three-dimensional, and compressible Navier–Stokes equations. The Navier–Stokes equations are discretized on arbitrary grid topologies using a cell-centered finite volume method. Second-order accuracy in space is achieved using the exact Riemann solver of Gottlieb and Groth [22], and least squares gradient calculations using QR factorization. In order to accelerate the convergence of the solution of the discretized system, a point-implicit method using analytic first-order inviscid and viscous Jacobians is used. A Newton sub-iteration method is used to improve time accuracy of the point-implicit method; the resulting method is second-order accurate in time. Tomaro et al. [59] converted the code from explicit to implicit, enabling CFL numbers as high as 10^6.

Cobalt is based on an arbitrary Lagrangian–Eulerian formulation and hence allows for all translational and rotational degree of freedom [27]. The code can simulate both free and specified Six Degree of Freedom (6DoF) motions, where rigid motion is specified from a motion input file. For rigid motion the location of a reference point on the aircraft is specified at each time step. In addition the rotation of the aircraft about this reference point is also defined using the rotation angles of yaw, pitch, and bank.

3. Test case

As a test case, the unsteady simulations of an NACA 0012 airfoil using *Cobalt* are considered. Both Euler and RANS meshes are available as shown in Fig. 2. In both meshes, the minimal distance from the body to each of the outer boundaries is $20c$, where c is the airfoil chord. The Euler mesh is generated using Gridgen version 15.0, and is a structured mesh generated by normal extrusion of surface connectors. The overview of the Euler mesh is shown in Fig. 2(a). The RANS mesh volume is rectangular with the airfoil geometry centrally located. The no-slip adiabatic wall boundary conditions is employed at the body surface, and a modified Riemann-invariant condition is implemented at the far-field boundary. The mesh consists of prisms and tetrahedra and was generated using SolidMesh 2D. Jirásek et al. [28] performed the sensitivity study of the grid size and time step. The pitch axis is set to $0.25c$, but the moment reference point is at the leading edge unless stated otherwise. The overview of the RANS mesh is shown in Fig. 2(b).

The steady Euler and RANS calculations are shown in Fig. 2. Note that Euler calculations are significantly faster than RANS (this is on the order of five in our calculations). The simulations correspond to $M_\infty = 0.3$ and $Re = 8.93 \times 10^6$ in order to match experimental data. All RANS simulations were performed using the Spalart–Allmaras (SA) turbulence model [52]. Both predictions compare well with the experiments at low angles of attack. The RANS model accurately predicts the maximum lift, but the stall region predictions do not match as well. The Euler model predicts the slopes of lift and pitch moment fairly well up to moderate angles of attack. Differences between the Euler predictions and experiments are observed at high angles of attack due to the inviscid assumption, although Euler simulations show flow separation on the upper surface at higher angle of attack resulting in a fall in lift

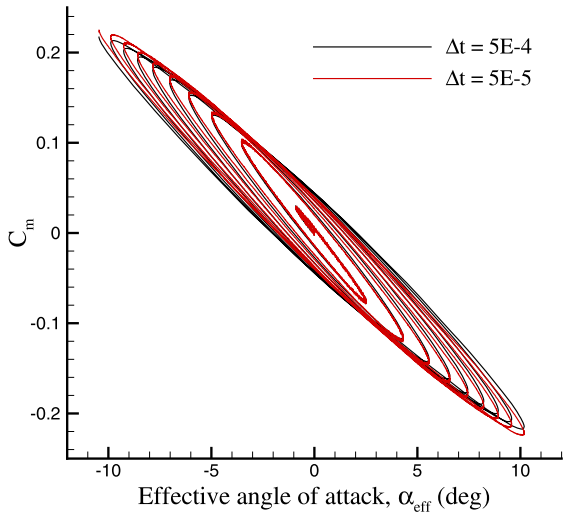

Fig. 3. Effect of time step size on pitch-moment coefficient for a chirp-plunge motion. Calculations were performed using Euler mode at $M_\infty = 0.3$.

slope. *Cobalt* used in Euler mode predicts the secondary boundary layer separation at high angles of attack due to adverse pressure gradients, however, these predictions are not accurate.

4. Results and discussions

4.1. Training RBFNN

The network used consists of a hidden radial basis layer with a Gaussian transfer function. All training data were generated using CFD with either the Euler or RANS equations. These solutions depend upon the time step size as shown in Fig. 3, in which the Euler calculations of pitch-moment for two chirp-plunge motions with different time step size are plotted. Both motions have an amplitude (H) of 0.5 m, an angular frequency (ω_h) of 2π rad/s, and started from a steady solution at zero degrees angle of attack. As the frequency of motion does increase with time, the differences become large at high and low effective angles of attack. These two maneuvers are used to approximate the effects of time step on the time-dependent aerodynamic loads. Six training datasets were defined to find a mapping between the normal force and pitch moment coefficients with the pitch and plunge motion variables at a fixed Mach number of 0.3. All motions have an initial frequency of 1 Hz, where the frequency is linearly increasing with time. The axial and vertical displacements are defined such that the Mach number remains constant with time.

The plunge motion has no rotation but the angle of attack changes due to the vertical displacements of the grid; this angle is named the "effective angle of attack" and is denoted by α_{eff} and is defined as:

$$\alpha_{\text{eff}} = \tan^{-1}\left(\frac{\dot{h}}{V}\right) \tag{13}$$

where V is the free-stream velocity. In total, six chirp motions were defined and started at different angles of attack as shown in Fig. 4. The starting angles of attack are $-5°$, $0°$ and $5°$ that allow us to include the effects of steady-state conditions into the pitching and plunging motions.

The following are some details of the network training using the CFD calculations. The vectors of time-dependent reduced frequencies are first calculated using the time gradients of pitch angles and vertical displacements, and next were normalized using the mean and standard deviation of each input. The data are then re-arranged according to Eq. (4) and the network performance is tested for different values of n, with a performance error threshold of 1×10^{-6}. All networks computed converged to the threshold error as shown in Fig. 5. The results showed that using $n = 4$ is sufficient for modeling the studied motions. The costs to train the networks and that of executing the networks for new maneuvers are around 88 s and 17 s, respectively.

4.2. Testing RBFNN

All six training motions were first simulated using the Euler equations in *Cobalt*. The CFD calculations started from a steady solution and ran for three seconds of physical time with a time step size of 5×10^{-5}, resulting in a total computational cost equivalent to that of 240 Euler steady-state calculations. Note that Euler calculations are five times faster than calculations using the RANS grid. Therefore, the cost of simulating all six training motions using Euler approach is equivalent to that of only 48 RANS steady-state calculations.

To provide network training data, the aerodynamic force and moment coefficients at each computational time step were extracted from the time-marching solutions. The force and moment

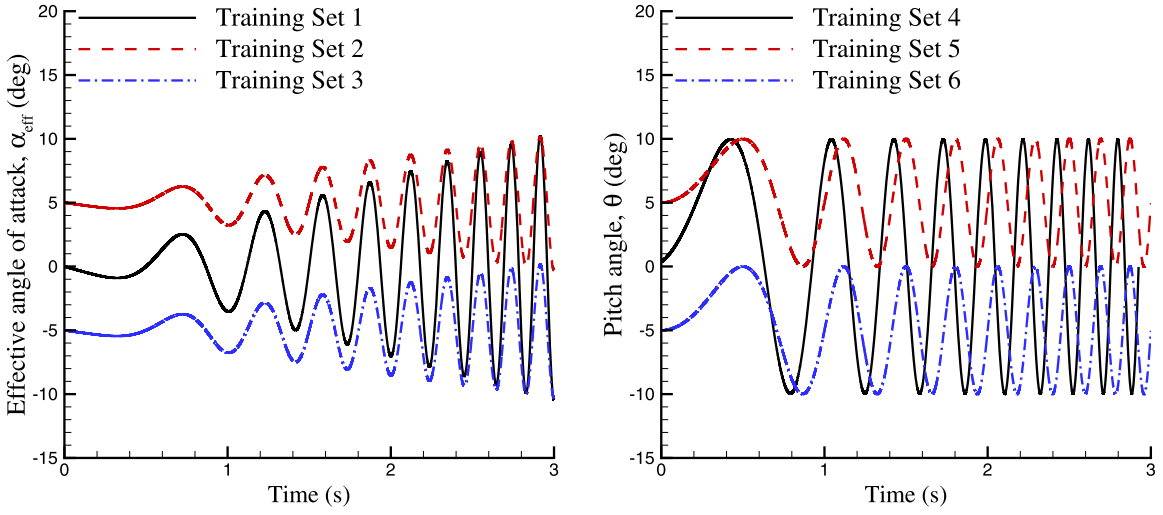

(a) Plunge training motions (b) Pitch training motions

Fig. 4. The plunge and pitch training maneuvers.

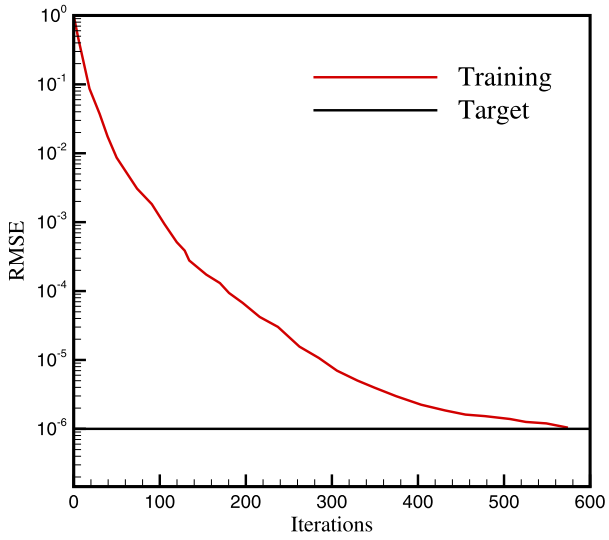

Fig. 5. RBF neural network training performance. The y-axis displays root mean squared error and the x-axis shows number of iterations.

axes are fixed in the computational space for the plunging motions, while it moves with the airfoil in pitch motions. This aids in obtaining the normal forces directly from the CFD solutions. The time-dependent normal force and pitch moment coefficients are compared in Fig. 6 for Training Sets 1 and 4. The figure shows that the amplitude of the coefficients is reducing for chirp-pitching and is increasing for chirp-plunging as motion time is increased. In the pitching motion, the frequency of motion increasing with time and therefore, the amplitude becomes smaller. A similar discussion applies to the plunging motion, but the increase in coefficients that result from the increase in the effective angle of attack overcomes the decrease due to the frequency increase.

The reported normal force and pitch moment coefficients were re-arranged similar to those described earlier. The data were then fed to the RBF neural network for training. Once the networks were trained, they were used to predict the aerodynamic loads for new maneuvers. The trained networks were tested for a number of motions. The results show that for most motion descriptions, the predicted ROM values agree well with the time-marching solutions. In one case, the ROM predictions showed large discrepancies as shown in Fig. 7, which shows the normal force coefficient corresponding to a plunge oscillation with a frequency of 1 Hz started at zero degrees angle of attack. The discrepancies are seen at the initial times where there is a jump in the normal force coefficient. This initial jump can be explained based on the energy of acoustic wave systems created by the initial grid perturbation [36,32]. The flow solutions of the moving airfoil at initial times are compared with the steady solution in Fig. 8. The figure shows a traveling wave in the flow as the grid starts to move vertically, resulting in a sudden fall of pressure in the lower section and a negative lift. As the shock moves, the lift suddenly starts to build up and results in a big jump in the angle-of-attack and normal force. The suddenly changing flow has $\dot{\alpha}$ values on the order of 100 larger than those used in the training data, and therefore results in an over-shoot problem for the network predictions. However, as the time was progressed the ROM predictions became closer to the time-dependent values. Such a jump in the normal force also occurs in the pitching motion but it is significantly smaller than the ones observed in the plunging motion [18]. In order to remedy this problem, the ROM predictions started just after the initial peak and results are compared with the time-marching solutions in Figs. 9(a) and 10(a) for normal force and pitch-moment coefficients. Figures show that the ROM predictions now match well with the time-marching calculations. The root mean square errors for predicted normal force and pitch moment are 0.0027 and 0.0045, respectively. Note that the cost of running the time-marching solution (full-order model) is around two wall-clock hours using 10 processors (2.3 GHz), while the ROM predictions take on the order of seconds.

Figs. 9(b) and 10(b) compare the ROM predictions for a ramp increase of angle of attack with a rate of 10 deg/s started at zero degrees angle of attack. Note that the forces and moments acting on the airfoil during translation are different from the static values as shown in Figs. 9(b) and 10(b). The flow change is not as fast as the angle of attack change, and hence the ramp motion underestimates the static coefficients. Figs. 9(b) and 10(b) show that ROM predictions agree well with the full-order simulation values ($\text{RMSE}_{C_N} = 0.004$ and $\text{RMSE}_{C_m} = 0.0045$). Also, two pitch oscillation motions with frequencies of $f = 0.5$ Hz and $f = 2.5$ Hz are considered. The low-frequency predictions are compared with the full-order model data in Figs. 9(c) and 10(c). Again a good match is found ($\text{RMSE}_{C_N} = 0.0069$ and $\text{RMSE}_{C_m} = 0.0042$). Likewise, Figs. 9(d) and 10(d) show that the ROM predictions closely match with the full-order simulations ($\text{RMSE}_{C_N} = 0.012$ and $\text{RMSE}_{C_m} = 0.0159$).

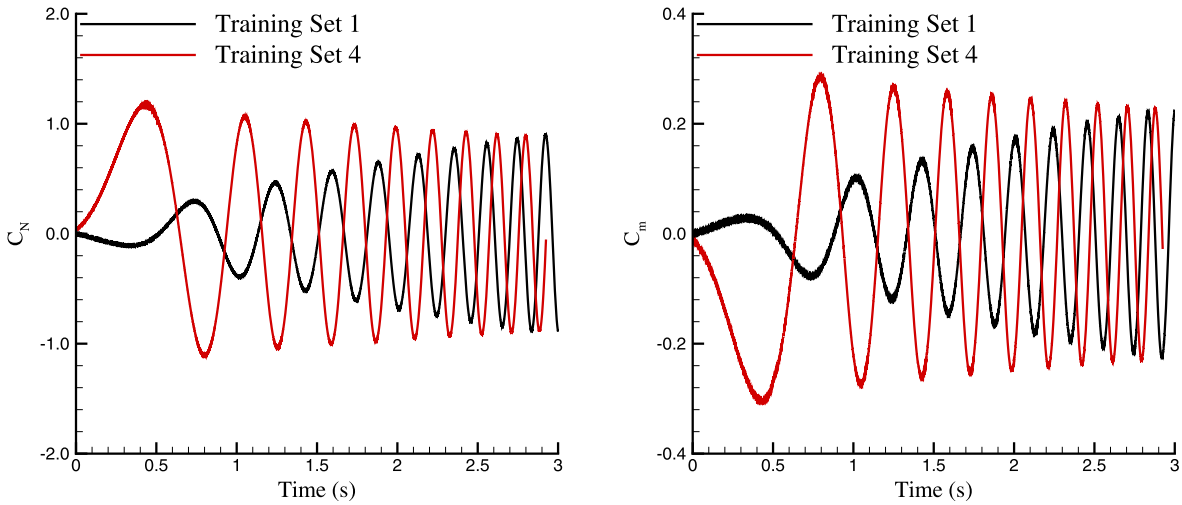

(a) Normal force coefficient (b) Pitching moment coefficient

Fig. 6. Simulation of training maneuvers using the Euler equations; $M = 0.3$.

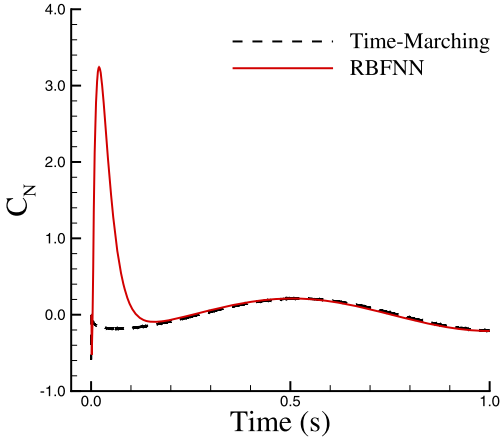

Fig. 7. Over-shooting of ROM predictions due to an initial jump. The motion is a constant-frequency plunge oscillation starting at zero degree angle of attack.

4.3. Using RBFNN for both primary and secondary data

The development of a ROM from RANS/Euler data is considered in this section. For network training purposes, these data are also called primary/secondary or "expensive/cheap" data, since the new ROM combines training data obtained from expensive and cheap sources. The cheap data are assumed to provide information at least about the trend of the target function, whereas the expensive calculations give quantitative information. To illustrate the approach the NACA 0012 airfoil is again used. The time-marching Euler predictions of all six training sets described in Fig. 4 are considered as cheap data. It is assumed that these predictions had similar trends to the RANS predictions, but with different values. The new RBF model tries to correct these trends by using much less expensive data.

In this paper, the expensive (or RANS) calculations were run only for two training sets. The first set is a chirp-pitch that runs for one second of physical time as shown in Fig. 11(a). The second set is a ramp motion with rate of 10 deg/s, started at -10° and runs for two seconds of physical time as shown in Fig. 11(b). Both motions have a sweep of angle of attack from the low to high angles, and therefore are found very helpful to learn the differences between Euler and RANS predictions. Both training sets were simulated using time-marching RANS equations and the SA turbulence model. Likewise the Euler predictions, a time step of 5×10^{-5} was used. For more details of time step selection, the reader is referred to the work of Cummings et al. [8]. This results in a computational cost equivalent to that of 40 RANS steady-state calculations and a total cost (both Euler and RANS) of 88 RANS steady-state calculations. Note that using RANS for time-marching simulations of all six training sets described in Fig. 4 will be equivalent to that of 240 steady-state calculations. In this sense, a ROM generated using both Euler and RANS calculations of maneuvers shown in Fig. 11

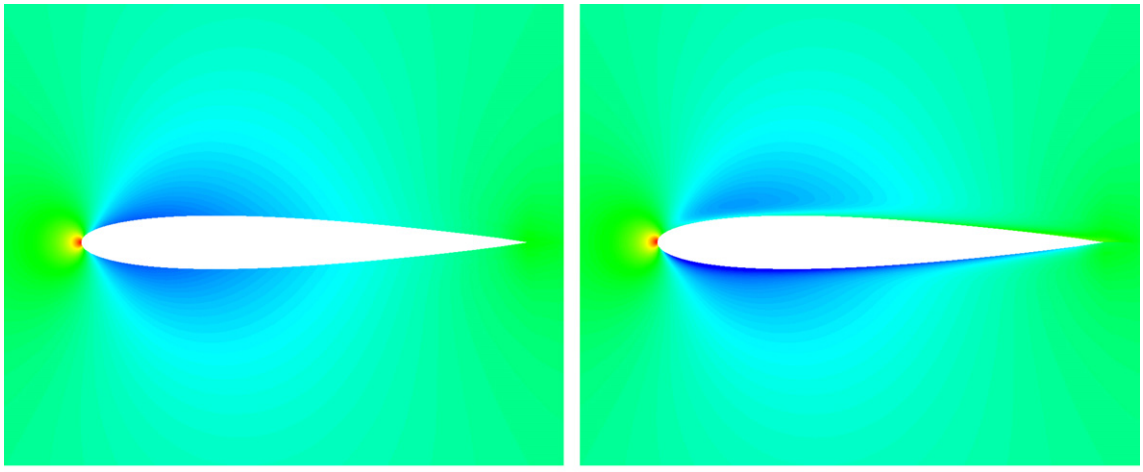

(a) Steady solution at α=0

(b) Plunge motion at $t = 5 \times 10^{-5}$ s

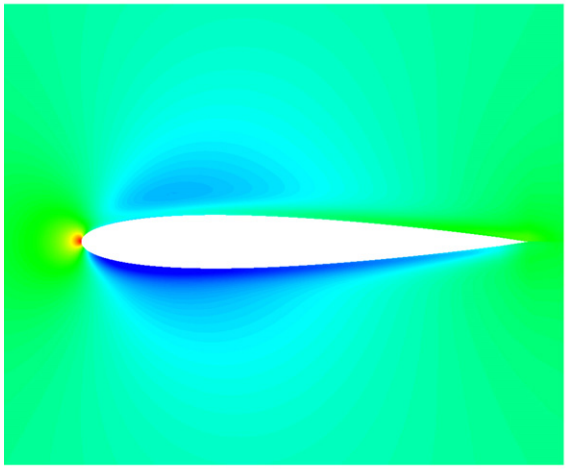

(c) Plunge motion at $t = 1 \times 10^{-4}$ s

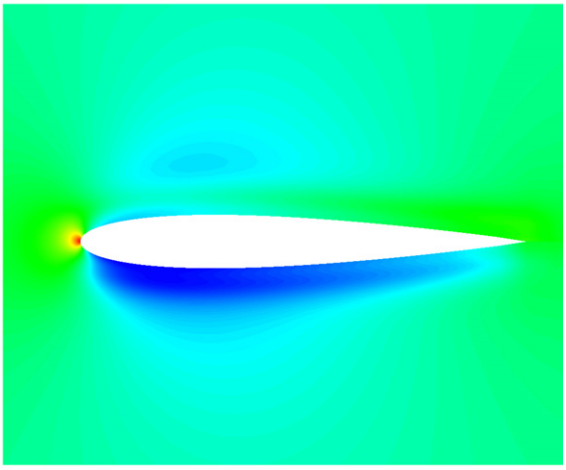

(d) Plunge motion at $t = 2 \times 10^{-4}$ s

Fig. 8. The flow-field pressure solution of plunge oscillation with $f = 1$ Hz at initial times; $M = 0.3$.

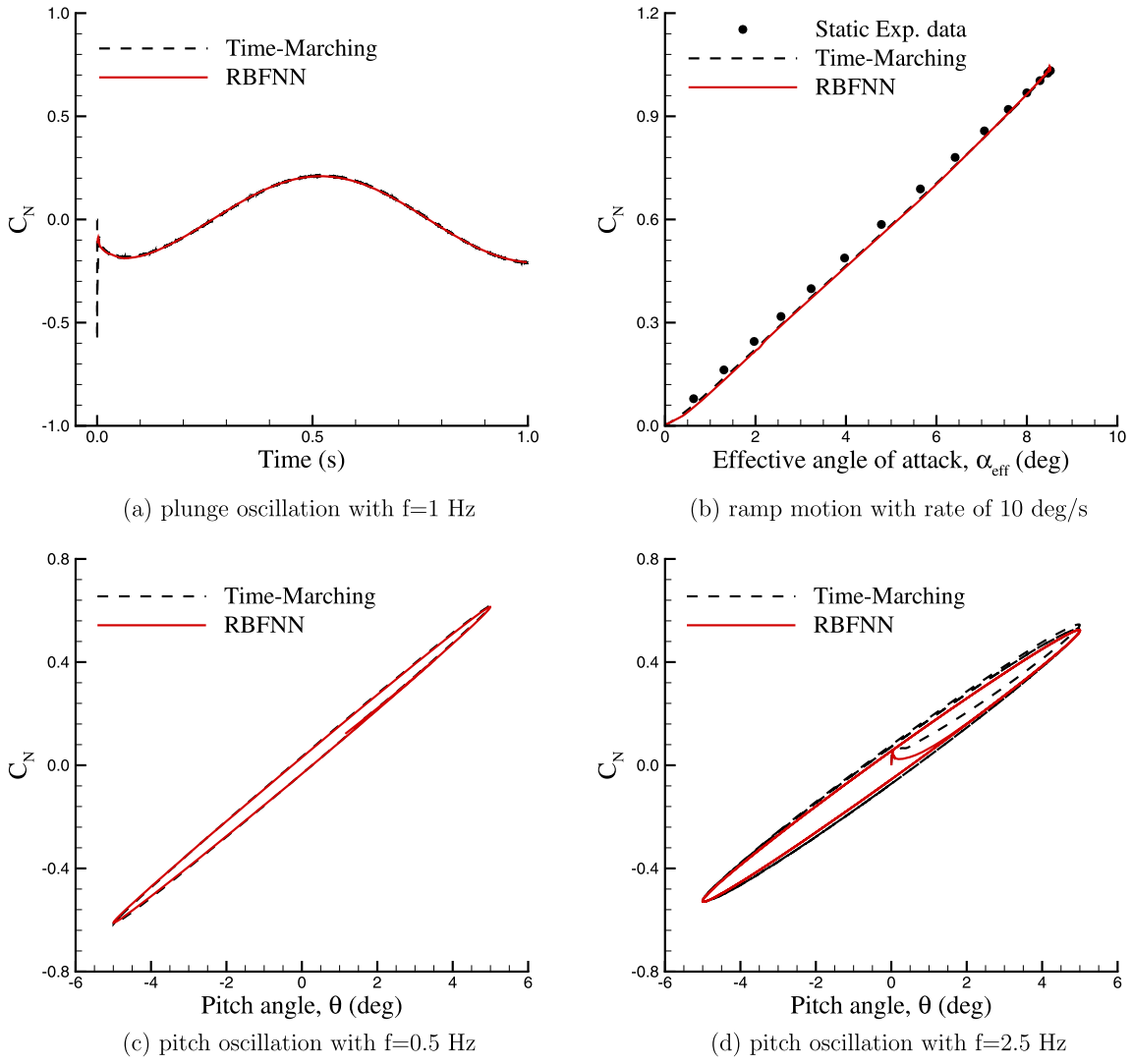

Fig. 9. RBF network predictions of normal force coefficients of testing motions; $M = 0.3$.

is 63% cheaper than a ROM generated using the RANS calculations of maneuvers shown in Fig. 4.

The RBFNN was trained for these maneuvers using both RANS and Euler evaluations and then was tested for new maneuvers. A pitch oscillation was used to demonstrate the network performance. The motion is a constant frequency type with $f = 0.5$ Hz started at zero degrees angle of attack. The unsteady normal force and pitch-moment coefficients were obtained using simulations of unsteady RANS equations and are shown in Figs. 12(a)–12(b) (called "time-marching"). Figs. 12(a)–12(b) show that the output of a network using both Euler and RANS training data match well with time-marching values. Such a network has similar trends as predicted by the network trained from Euler data and then corrects them. The network using only Euler data match time-marching solutions at low angles of attack, but overestimates the values at high angles due to the inviscid assumption. Figs. 12(a)–12(b) show that using only the RANS training maneuvers shown in Fig. 11 does not help much to approximate the time-marching values, since these maneuvers are short and do not properly cover the frequency and starting angle of attack space. Note that the input/output mapping used in this paper can be extended to include the effects of varying freestream Mach number as well. As an example, the primary and secondary training motions were simulated at $M = 0.6$ and used for creating a ROM. Figs. 13(a) and 13(b) show that ROM predictions at $M = 0.6$ also agree well with the full-order simulation values of normal force and pitch moment.

5. Conclusions

A framework for the use of Radial Basis Function Neural Networks for the generation of nonlinear and unsteady aerodynamic simulations using Euler and RANS is presented. Once the network is trained, it can predict the unsteady aerodynamic loads from motion descriptions on the order of few seconds. The test case used was an airfoil undergoing pitching and plunging motions. A mapping between the predictions of unsteady normal force and pitch-moment coefficients and the motion amplitude and reduced frequency was described. The paper then extended this mapping to include both Euler and RANS predictions. The solution of RANS equations provide the quantitative and qualitative solution of flow around aircraft, although they are expensive in terms of computational resources. The Euler simulations are less expensive and provide qualitative data up to moderate angles of attack. The combination of both predictions in this new model aids in correcting the Euler trends by using much less RANS data, and therefore is very helpful for applications that would require excessive CFD calculations.

In respect to training data, the design of special maneuvers which can capture a broad spectrum of physical phenomena within

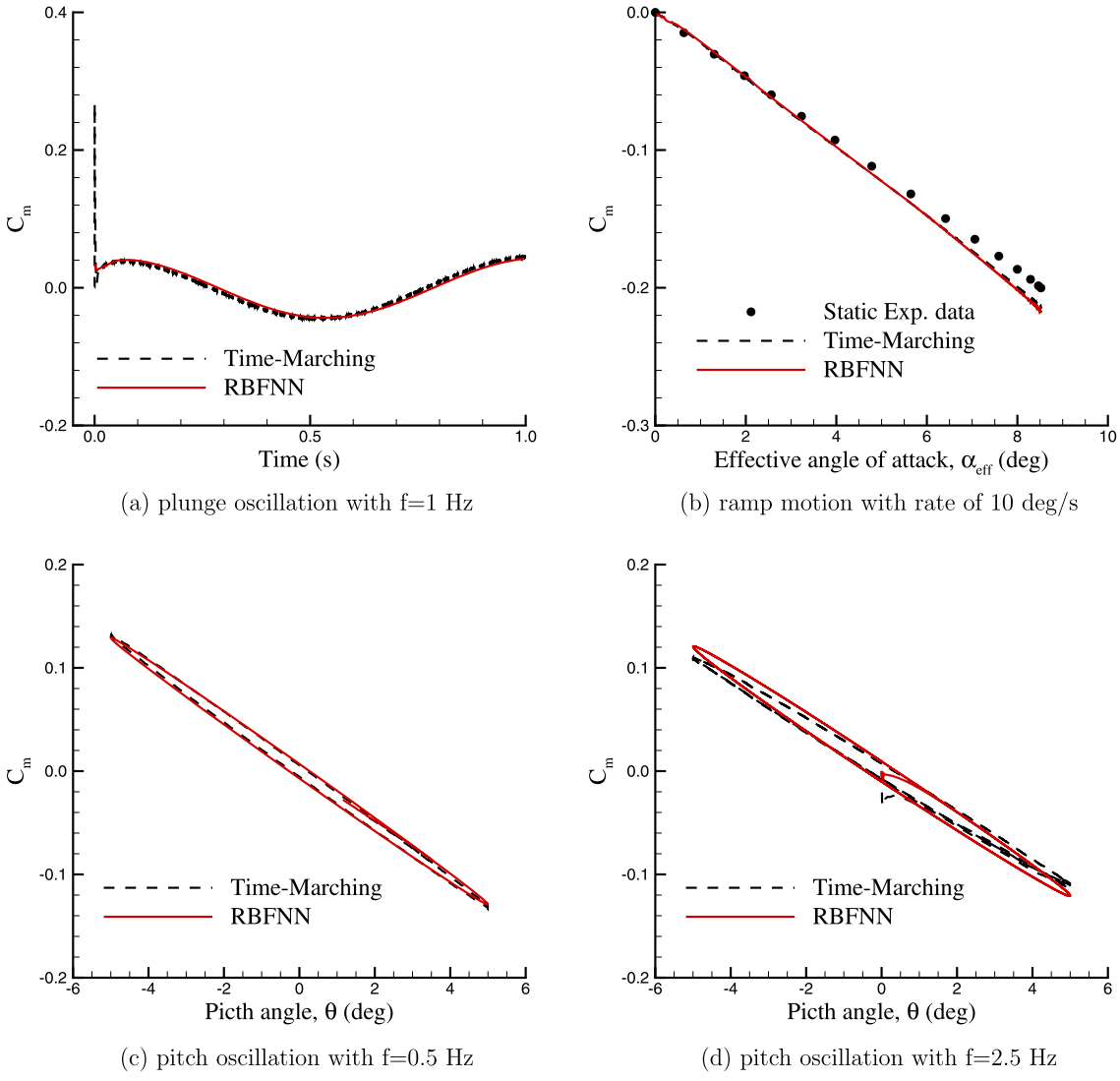

(a) plunge oscillation with f=1 Hz

(b) ramp motion with rate of 10 deg/s

(c) pitch oscillation with f=0.5 Hz

(d) pitch oscillation with f=2.5 Hz

Fig. 10. RBF network predictions of pitch-moment coefficients of testing motions; $M = 0.3$.

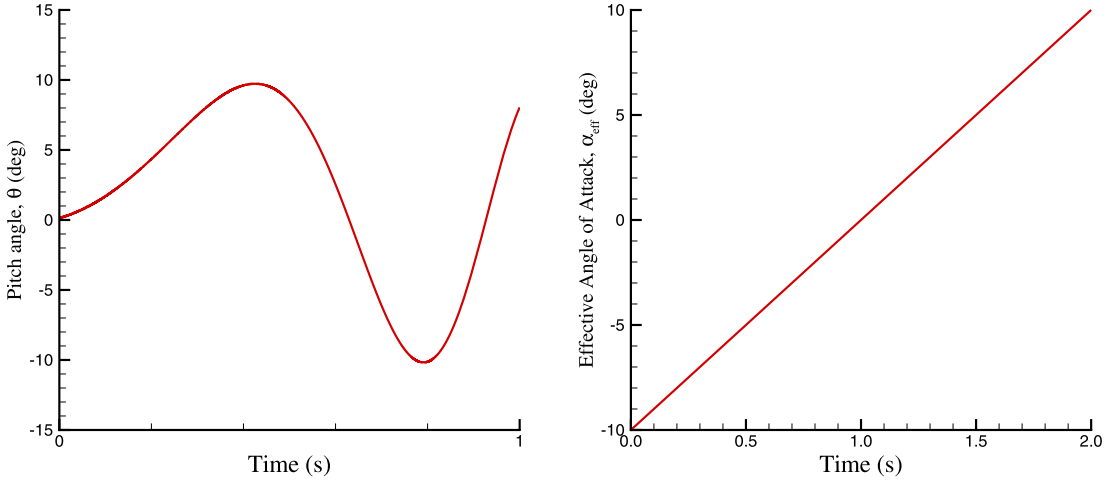

(a) Pitching motion

(b) Ramp motion

Fig. 11. Training data for RANS simulations; $M = 0.3$.

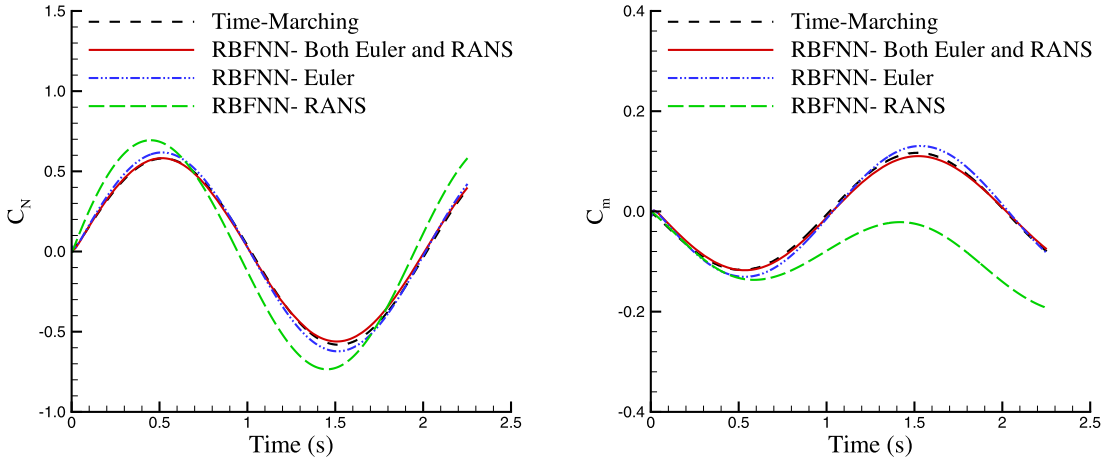

(a) Normal force coefficient (b) Pitching-moment coefficient

Fig. 12. RBFNN predictions using both Euler and RANS equations; $M = 0.3$.

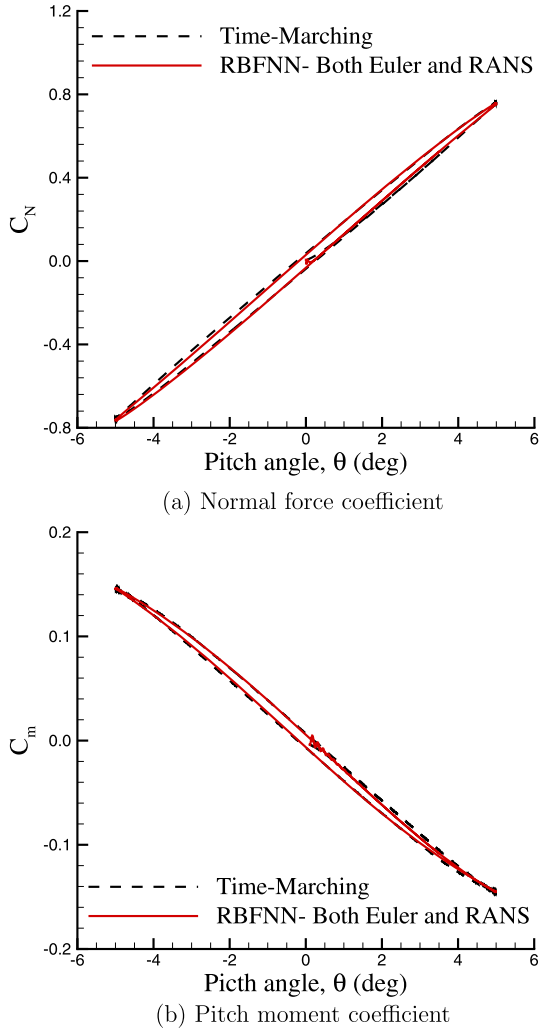

(a) Normal force coefficient

(b) Pitch moment coefficient

Fig. 13. RBFNN predictions using both Euler and RANS equations. The motion is $\alpha = 5^\circ \sin(\omega t)$ with $f = 0.5$ Hz and $M = 0.6$.

the relevant regressor space helped to define only six training maneuvers. This is a very substantial reduction compared with classical design of experiment methods. The maneuvers are frequency-sweep types started at different angles of attack. The unsteady Euler simulation of these training maneuvers were then used to generate reduced order models, which were then used to approximate unsteady loads of new motion in a fraction of a few seconds. A number of pitch and plunge motions were then used to demonstrate the network performance. The results showed that RBFNN predictions matched well with the full-order simulations. For plunge oscillations, an initial jump was observed in the predictions. This initial jump can be explained based on the energy of acoustic wave systems created by the initial grid perturbation; such a jump resulted in an over-shooting problem in the network predictions.

Having demonstrated the capability of RBFNN for predictions of unsteady aerodynamic loads, the paper then presented an approach to find a mapping between unsteady viscous loads and motion variables using many Euler and few RANS training data. Only two relatively short motions were simulated using the RANS equations, which reduced the total computational cost by around 63% compared with RANS calculation of all six training maneuvers. Results showed that the networks trained by both Euler and RANS simulations closely follow the full-order simulation of new motions, while a network using only RANS predictions did not match well, since only two short motions were considered. This framework also can be applied to combine training data from small and large time step size. Future work will include investigating the use of other training maneuvers such as Spiral, Schroeder, doublet, etc., and testing the framework at transonic speeds. The input vector will be extended to include the freestream Mach number for creating ROMs that could predict aerodynamic responses in the angle-of-attack/Mach/frequency space.

Acknowledgements

Mehdi Ghoreyshi and Adam Jirásek were supported by the National Research Council/US Air Force Office of Scientific Research. Their financial support is gratefully acknowledged. The authors appreciate the support provided by the Modeling and Simulation Research Center at USAFA.

References

[1] M.J. Abzug, E.E. Larrabee, Airplane Stability and Control: A History of the Technologies That Made Aviation Possible, Cambridge University Press, Cambridge, 2002.
[2] M.A. Arbib, The Handbook of Brain Theory and Neural Networks, second edition, MIT Press, 2003.
[3] R. Babuska, Fuzzy Modeling for Control, Kluwer Academic Publishers, Norwell, 1998.

[4] W.F. Ballhaus, P.M. Goorjian, Computation of unsteady transonic flows by indicial methods, AIAA Journal 16 (2) (1978) 117–124.
[5] G.H. Bryan, Stability in Aviation, MacMillan, London, 1911.
[6] B.D. Buhmann, Radial basis functions, Acta Numerica 9 (2000) 1–38.
[7] W.A. Cowley, H. Glauert, The effects of the lag of the downwash on the longitudinal stability of an airplane and on the rotary derivative M_q, NASA TM-654, R.&M.-718, February 1912.
[8] R.M. Cummings, S.A. Morton, D.R. McDaniel, Experiences in accurately predicting time-dependent flows, Progress in Aerospace Sciences 44 (2008) 241–257.
[9] T.S. Deisboeck, J.Y. Kresh, Complex Systems Science in Biomedicine, Springer, USA, 2006.
[10] W.E. Faller, S.J. Schreck, Real-time prediction of unsteady aerodynamics: application for aircraft control and maneuverability enhancement, IEEE Trans. Neural Networks 6 (6) (1995) 1461–1468.
[11] W.E. Faller, S.J. Schreck, Neural networks: applications and opportunities in aeronautics, Progress in Aerospace Sciences 32 (5) (1996) 433–456.
[12] J.R. Forsythe, K.A. Hoffmann, R.M. Cummings, K.D. Squires, Detached-eddy simulation with compressibility corrections applied to a supersonic axisymmetric base, Journal of Fluids Engineering 32 (4) (2002) 911–923.
[13] R. Forsythe, K.D. Squires, K.E. Wurtzler, P.R. Spalart, Detached-eddy simulation of fighter aircraft at high alpha, Journal of Aircraft 41 (2) (2004) 193–200.
[14] J.R. Forsythe, S.H. Woodson, Unsteady computations of abrupt wing stall using detached-eddy simulations, Journal of Aircraft 42 (3) (2005) 606–616.
[15] A. Gaitonde, D.P. Jones, Reduced order state-space models from the pulse responses of a linearized CFD scheme, International Journal of Numerical Methods in Fluids 42 (6) (2003) 581–606.
[16] M. Ghoreyshi, K.J. Badcock, A.D. Ronch, A. Swift, S. Marques, N. Ames, Framework for establishing the limits of tabular aerodynamic models for flight dynamics analysis, Journal of Aircraft 48 (1) (2011) 42–55, also AIAA Paper 2009-6273, August 2009.
[17] M. Ghoreyshi, K.J. Badcock, M.A. Woodgate, Accelerating the numerical generation of aerodynamic models for flight simulation, Journal of Aircraft 46 (3) (2009) 972–980, also AIAA Paper 2009-733, January 2009.
[18] M. Ghoreyshi, A. Jirásek, R.M. Cummings, A computational investigation into the use of response functions for aerodynamic loads modeling, AIAA Journal 50 (6) (2012) 1314–1327, also AIAA Paper 2011-3518, January 2011.
[19] B. Glaz, L. Liu, P.P. Friedmann, Reduced-order nonlinear unsteady aerodynamic modeling using a surrogate-based recurrence framework, AIAA Journal 48 (10) (2010) 2418–2429.
[20] M.G. Goman, A.N. Khrabov, State-space representation of aerodynamic characteristics of an aircraft at high angles of attack, AIAA Paper 92-4651, August 1992.
[21] S. Görtz, D. McDaniel, S.A. Morton, Towards an efficient aircraft stability and control analysis capability using high-fidelity CFD, AIAA Paper 2007-1053, January 2007.
[22] J.J. Gottlieb, C.P.T. Groth, Assessment of Riemann solvers for unsteady one-dimensional inviscid flows of perfect gasses, Journal of Computational Physics 78 (2) (1998) 437–458.
[23] D.I. Greenwell, A Review of unsteady aerodynamic modelling for flight dynamics of maneuverable aircraft, AIAA Paper 2004-5276, August 2004.
[24] K.C. Hall, J.P. Thomas, E.H. Dowell, Reduced-order modelling of unsteady small-disturbance using a frequency-domain proper orthogonal decomposition technique, AIAA Paper 1999-655, January 1999.
[25] R.V. Jategaonkar, Flight Vehicle System Identification, AIAA Educational Series, AIAA, Reston, 2006.
[26] T. Jeans, D. McDaniel, R.M. Cummings, W. Mason, Aerodynamic analysis of a generic fighter using delayed detached-eddy simulations, Journal of Aircraft 46 (4) (2009) 1326–1339.
[27] A. Jirásek, R.M. Cummings, Reduced order modelling of X-31 wind tunnel model aerodynamic loads, AIAA Paper 2010-4693, June–July 2010.
[28] A. Jirásek, T.L. Jeans, M. Martenson, R.M. Cummings, K. Bergeron, Improved methodologies for maneuver design of aircraft stability and control simulations, AIAA Paper 2010-515, January 1999.
[29] S.G. Krantz, H.R. Parks, The Implicit Function Theorem: History, Theory, and Applications, Birkhäuser, Boston, 2002.
[30] H.G.K. Küssner, Stresses produced in airplane wings by gusts, NASA TM-654, January 1932.
[31] C.L. Ladson, Effects of independent variation of Mach and Reynolds number on the low-speed aerodynamic characteristics of NACA0012 airfoil section, NASA Technical Paper 4074, January 1988.
[32] L.G. Leishman, Indicial lift approximations for two-dimensional subsonic flow as obtained from oscillatory measurements, Journal of Aircraft 30 (3) (1993) 340–351.
[33] A.U. Levin, K.S. Narendra, Control of nonlinear dynamical systems using neural networks: controllability and stabilization, IEEE Trans. Neural Networks 4 (2) (1993) 192–206.
[34] R. Liebe, Flow Phenomena in Nature: A Challenge to Engineering Design, WIT Press, Great Britain, 2007.
[35] P. Lisandrin, G. Carpentieri, M. van Tooren, Investigation over CFD-based models for the identification of nonlinear unsteady aerodynamics responses, AIAA Journal 44 (9) (2006) 2043–2050.
[36] H. Lomax, Indicial aerodynamics, in: AGARD Manual of Aeroelasticity, Part II, 1960, Chapter 6.
[37] D.J. Lucia, P.S. Beran, W.A. Silva, Reduced-order modeling: new approaches for computational physics, Progress in Aerospace Sciences 40 (1) (2004) 51–117.
[38] F.D. Marques, J. Anderson, Identification and prediction of unsteady transonic aerodynamic loads by multi-layer functionals, Journal of Fluids and Structure 1 (6) (2011) 83–106.
[39] M. McKay, R.J. Beckman, W.J. Conover, A comparison of three methods for selecting values of input variables in the analysis of output from a computer code, Technometrics 21 (2) (1979) 239–245.
[40] E.A. Morelli, Real time parameters estimation in the frequency domain, AIAA Paper 99-4043, August 1999.
[41] E.A. Morelli, System identification programs for aircraft (SIDPAC), AIAA Paper 2002-4704, August 2002.
[42] S.A. Morton, J.R. Forsythe, A.M. Mitchell, D. Hajek, Detached-eddy simulations and Reynolds-averaged Navier–Stokes simulations of delta wing vortical flowfields, Journal of Fluids Engineering 124 (4) (2002) 924–932.
[43] P.C. Murpy, V. Klein, Validation of methodology for estimating aircraft unsteady aerodynamics parameters from dynamic wind tunnel tests, AIAA Paper 2003-5397, August 2003.
[44] F.E. Olcer, J.V.R. Prasad, L.N. Sankar, J.J. Bain, J. Zhao, C. He, Development and evaluation of reduced order models of on-blade control for integrated flight and rotor control, in: Proceedings of the American Helicopter Society, 66th Annual Forum, Phoenix, Arizona, May 2010.
[45] C. O'Neill, A. Arena, Time domain training signals comparison for computational fluid dynamics based aerodynamic identification, Journal of Aircraft 42 (2) (2005) 421–428.
[46] N.V. Queipo, R.T. Haftka, W. Shyy, T. Goel, R. Vaidyanathan, P.K. Tucker, Surrogate-based analysis and optimization, Progress in Aerospace Sciences 41 (1) (2005) 1–28.
[47] T.D. Robinson, M.S. Eldred, K.E. Willcox, R. Haimes, Surrogate-based optimization using multifidelity models with variable parameterization and corrected space mapping, AIAA Journal 46 (11) (2008) 2814–2822.
[48] W.R. Sears, Some aspects of non-stationary airfoil theory and its practical applications, Journal of the Aeronautical Sciences 8 (5) (1941) 104–108.
[49] W.A. Silva, R.E. Bartels, Development of reduced-order models for aeroelastic analysis and flutter prediction using the CFL3Dv6.0 code, Journal of Fluids and Structure 19 (6) (2004) 729–745.
[50] T.W. Simpson, D. Poplinski, P.N. Koch, J.K. Allen, Metamodels for computer-based engineering design: survey and recommendations, Engineering with Computers 17 (2) (2001) 129–150.
[51] G.M. Sirouris, Missile Guidance and Control Systems, Springer-Verlag, New York, 2004.
[52] P.R. Spalart, S.R. Allmaras, A one equation turbulence model for aerodynamic flows, AIAA Paper 1992-0439, January 1992.
[53] V.J.E. Stark, Indicial coefficients for a cropped delta wing in incompressible flow, Journal of Aircraft 23 (5) (1985) 370–375.
[54] W.Z. Strang, R.F. Tomaro, M.J. Grismer, The defining methods of Cobalt: a parallel, implicit, unstructured Euler/Navier–Stokes flow solver, AIAA Paper 1999-0786, 1999.
[55] M. Tobak, G.T. Chapman, Nonlinear problems in flight dynamics involving aerodynamic bifurcations, NASA TN-86706, 1985.
[56] M. Tobak, G.T. Chapman, L.B. Schiff, Mathematical modeling of the aerodynamic characteristics in flight dynamics, NASA TN-85880, 1984.
[57] M. Tobak, L.B. Schiff, Generalized formulation of nonlinear pitch–yaw–roll coupling: Part 1: Nonaxisymmetric bodies, AIAA Journal 13 (3) (1975) 323–326.
[58] M. Tobak, L.B. Schiff, Generalized formulation of nonlinear pitch–yaw–roll coupling: Part 2: Nonlinear coning-rate dependence, AIAA Journal 13 (3) (1975) 327–332.
[59] R.F. Tomaro, W.Z. Strang, L.N. Sankar, An implicit algorithm for solving time dependent flows on unstructured grids, AIAA Paper 1997-0333, 1997.
[60] H. Wagner, Über die Entstehung des dynamischen Auftriebes von Tragflügeln, Zeitschrift für angewandte Mathematik und Mechanik 1 (1) (1925) 17–35.